ELSEVIER

Nuclear Instruments and Methods in Physics Research B 184 (2001) 458–465

NIM B
Beam Interactions with Materials & Atoms

www.elsevier.com/locate/nimb

Diagnostics of gas density gradient by swift ions

D. Gardès [a,*], G. Maynard [b], G. Belyaev [c], I. Roudskoy [c]

[a] *Institut de Physique Nucléaire, BP no. 1, IPN-IN2P3, F-91406 Orsay Cedex 2, France*
[b] *Laboratoire de physique des gaz et des plasmas, LPGP, Université Paris-sud, F-91405 Orsay Cedex 2, France*
[c] *Institute for Theoretical and Experimental Physics, ITEP Moscow, 117259, Russia*

Received 19 June 2001; received in revised form 17 July 2001

Abstract

Measurements of density gradients resulting from gas ejection through a small aperture are presented. Fluorescence emission light from gas atoms excited by a fully stripped 60 MeV carbon beam was used as a diagnostic tool. The experimental results showed good agreement with the data of a hydrodynamic simulation. This work is related to the design of a high-pressure target enclosed by two fast valves in order to investigate the so-called density effect in ion stopping experiments [Nucl. Instr. and Meth. B 164–165 (2000) 139]. © 2001 Published by Elsevier Science B.V.

Keywords: 34.50.Bw; 32.50.+d; 07.35.+k

1. Introduction

The so-called density effect in stopping power is a long-standing problem [1], already investigated experimentally by Geissel et al. [2] and Bimbot [3]. A new experimental approach, which involves a high-pressure gas target including a density variation (same area density but variation in length) is under development.

In the MeV/u energy regime, when the target density is increased by a factor of 100, the energy lost by a heavy ion beam can be modified by a few tens of percent. The determination of the variation with target density of the charge dependent stopping cross-section of heavy ions will provide new valuable information for the ion–matter interaction process. However, to be effective such an experiment requires to satisfy several drastic requirements for the target design: the basic one is a possibility to change the density of the target at least by a factor of 10 ($n_e = 5.4 \times 10^{18}$–5.4×10^{19} cm^{-3}) during the experiment, keeping constant the linear density. Next, the coupling of the high-pressure container with the vacuum of the accelerator must be as little disturbing as possible especially for the charge state measurements. To obtain the required abrupt pressure gradient at both ends of the target, a fast valve system has been proposed [4]. Using this device, we observed that quasi-stationary gas flows with density gradients along the beam axis arise about 100 μs after opening of the valves. These flows can introduce

* Corresponding author. Tel.: +33-1-69-15-72-17; fax: +33-1-69-15-45-07.
E-mail address: gardes@ipno.in2p3.fr (D. Gardès).

0168-583X/01/$ - see front matter © 2001 Published by Elsevier Science B.V.
PII: S0168-583X(01)00785-6

an error in the experimental determination of the linear density and can also affect the final charge state of the incoming ions. Therefore, a precise measurement of the density gradient at both ends of the target has to be performed in order to calibrate this source of perturbation.

In the present work we present the results of a density gradient diagnostic behind the new fast valve rotating system, which is described below. A beam of C^{6+} ions obtained by stripping of a 60 MeV C^{5+} beam delivered by the Orsay Tandem accelerator was used as a probe to excite the gas scintillation. This method allows to measure with a high spatial resolution the density of the gas during its stationary regime of leakage. The nature of the scintillating gas has been chosen in order to fit this application. The use of fully ionized ions at high enough energy for the recombination process to be negligible, enabled us to leave out an additional analysis of the dependence of the light emission on the ion charge states.

2. Experimental set-up

For the diagnostic application a simplified version of the gas target was used. The gas vessel was closed in one end by a 6 μm aluminum foil and in the other by the rotating fast valve system (Fig. 1). The geometry of the aperture of the valve has been specially designed to reduce the exit conductance length. In this particular experimental configuration the output conductance consists in a 1.6 mm diameter and 0.7 mm length cylinder in front of a 2 mm diameter, 2 mm length hole (Fig. 1). The rotor of the rotating system was set in motion by a pulse solenoid. The aperture time response of the valve was measured using light transmission of a laser beam. The result is shown in Fig. 2. The characteristic property of the valve was a 1 ms time interval during which the aperture remained entirely open and allows the full transmission of a beam pulse of the same duration without interference.

The entrance aluminum foil played two roles. It cuts off the gas container from the vacuum beam line and it strips 60 MeV, C^{5+} ions to the bare nuclei.

The direct light of the gas fluorescence was collected on the CCD of an intensified camera via a standard optical device (28 mm, F1.4) [5]. The intensifier consisted of a photocathode, a microchannel plate electron multiplier and a phosphor positioned in front of the CCD array. The spectral range of the photocathode extends from 200 to 820 nm. Image processing software (WinView software

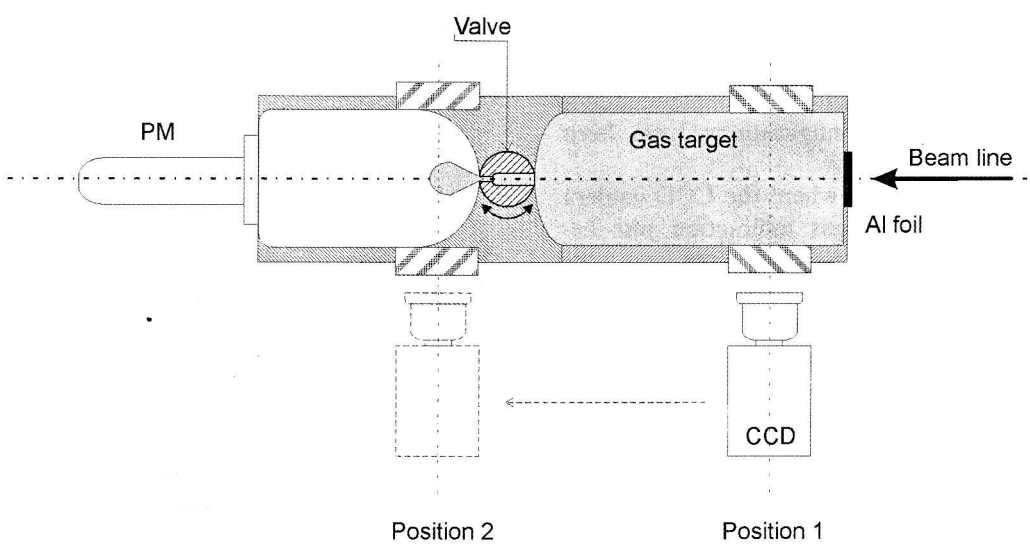

Fig. 1. Experimental configuration for ejection gas measurements.

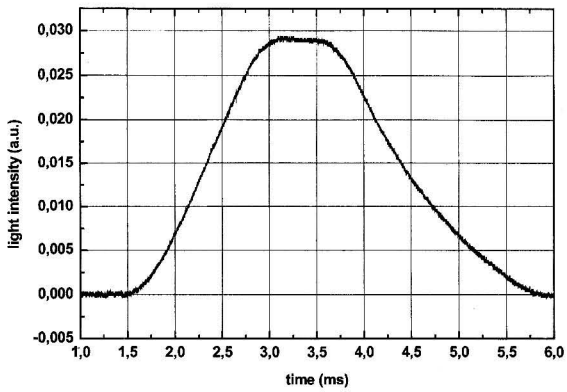

Fig. 2. Aperture time response of the fast valve.

[5]) allowed to display in pseudo color palette the intensity levels recorded by the CCD camera and the basic processes of the image (background subtraction, ASCII transformation, etc.)

In addition, a photomultiplier (PM) located behind the target was used for monitoring the beam intensity and pulse duration. The quartz window of the PM was used as a scintillator. The linearity of its dynamic range (~10) was checked with a Faraday cup (FC) in a preliminary experiments without gas. We use a PM because it works (unlike FC) in the proper way in a gaseous medium. The signal from the PM was recorded by a digital oscilloscope Lecroy-9304A with subsequent transformation into ASCII format for later processing. This information has been used for normalizing the gas fluorescence with respect to the number of incident ions.

Two experimental configurations have been used in the work:

1. The calibration mode, where the CCD camera looked at the beam–gas interaction just below the first metallic window (position 1 in Fig. 1).
2. The measurement mode, where the camera was watching the ejection area of the fast valve (position 2).

The first position was used to establish the correlation between the light yield and the gas pressure for a given ion beam intensity in steady state. The second one allowed to analyze the density gradient in a gas flow resulting from the gas leakage through a small aperture of the valve.

Two gases in a wide range of pressures (1–700 Torr) have been investigated, i.e. hydrogen which is of interest for use with the fast valve system and neon for its scintillating properties.

3. Calibration processes and theoretical considerations

The carbon beam was pulsed with a pulse duration of 1 ms for hydrogen gas and 300 μs for Ne experiments. Results of measurements are presented in Figs. 3 and 4, respectively. From these

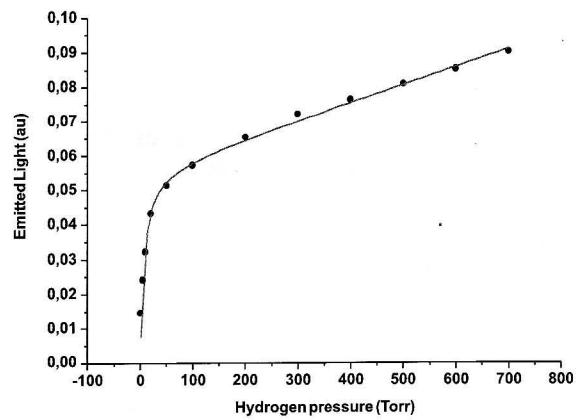

Fig. 3. Dependence of emission light with gas pressure for hydrogen. Solid line corresponds to Eq. (6).

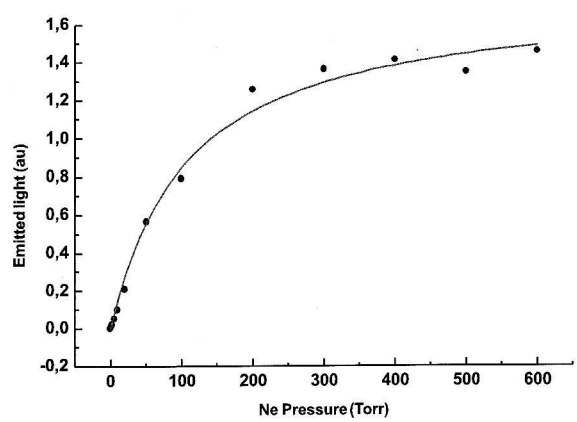

Fig. 4. Dependence of emission light with gas pressure for neon. Solid line corresponds to Eq. (2).

figures, we see that the intensity of the emission of light first increases linearly with target density at low pressure. This occurs for pressure less than 5 Torr in hydrogen and 50 Torr in neon. Above these pressures, the two curves exhibit slightly different behaviors. In neon the emission tends to saturate at high pressure while in hydrogen it still increases linearly but with a much smaller slope than at low pressure. Such behavior of the calibration curves can be analyzed by looking at the collisional-radiative rate equations leading to light emission. For our calibration purpose, we do not need to go into the detail of all the microscopic processes, so we present below a qualitative description of the emission process.

As the beam intensity is rather small, the population of excited or ionized atom/molecule is small enough for neglecting all collision between two excited or ionized atoms and the incident beam interacts only with the gas particles in their ground state. The non-linear dependence of light emission with gas pressure can then be related to the competition between the lifetime of the radiative excited states and the inverse of the frequency for the collision reactions leading to quenching of these radiative states. It is well known that radiative transitions are not the only processes that can lead to decay of the excited states of gas atoms. In dense gases the collision mechanism have to be taken into consideration. An important point of our experiment is that the resonance lines, that can be absorbed by the ground state of the gas particles, do not contribute to the detector signal as their wavelength are well below 200 nm. Therefore, the absorption plays a negligible role and the detector signal is directly connected to the number of emission events.

With 60 MeV carbon ions we are in the high velocity Bethe regime. Therefore the excitation cross-sections are nearly proportional to the optical oscillator strength of the transition and inversely proportional to the excitation energy. From these rules we can deduce that the ionization and excitation processes are of equal importance and nearly half of the ionization processes produce electrons with a kinetic energy larger than the ionization potential. As a result many highly excited states are created either from the direct beam–atom interaction or from the secondary electrons. These excited states contribute further to the light emission through a cascade of radiative decay.

The simplest way to introduce the influence of collisions is to suppose only one-step processes. That is, a radiative state, once produced, will either emit a photon or be destroyed by collision. Each radiative state i is then characterized by a creation coefficient τ_i, a coefficient for spontaneous emission A_i and a coefficient D_i for destruction by collisions. By equaling the rate of creation and destruction, we obtain the equilibrium condition

$$n_g n_B \tau_i = A_i n_i + D_i n_i n_g, \tag{1}$$

with n_g, n_B and n_i the density of the gas particles, the incoming carbon ions and the radiative state, respectively. By supposing that the most intense lines have coefficients of the same order of magnitude, this gives an emission intensity of the form

$$I = \frac{kP}{P_0 + P}, \tag{2}$$

with P the gas pressure in Torr and $P_0 = 3.14 \times 10^{-23}$ A/D.

Eq. (2) was used to fit the experimental points in the neon case. The solid line in Fig. 4 corresponds to the value $P_0 = 107.6$ Torr. Note that it is not possible to reproduce the hydrogen data, using Eq. (2). The value of P_0 may be related to microscopic coefficients: in neon, the probability for decay of the most intensive lines observed in the experiment is in the range $(1–3) \times 10^8$ s^{-1} [8], while the frequency of atom collisions for quenching was found to be 6×10^6 s^{-1} under a gas pressure of 1 Torr [6], the quenching process being essentially due to the reaction

$$Ne^* + Ne \rightarrow Ne_2^+ + e. \tag{3}$$

The probabilities of radiation and collision processes are then getting equal when the gas pressure reaches approximately 50 Torr. This is in reasonable agreement with our P_0 value, taking into account the approximations used to derive Eq. (2).

The effect of the quenching collisions can be clearly identified by using a gas mixture $H_2 + Ne$. In Fig. 5 we report the variation of intensity with

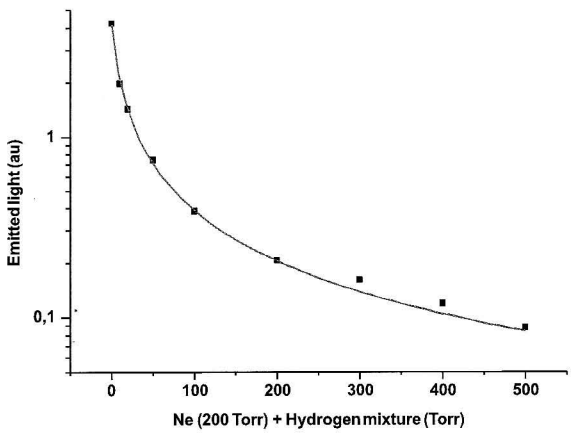

Fig. 5. Dependence of emission light with gas pressure for a mixture neon + hydrogen. The pressure of Ne is kept constant at 200 Torr. The pressure scale indicates the sum Ne + H. Solid line corresponds to Eq. (5).

increasing the hydrogen pressure, keeping constant the Ne partial pressure. As observed experimentally, the emission comes mainly from the neon atoms. Therefore by introducing the hydrogen gas we only increase the destruction rate due to collisions of the radiative neon states: as the energy of the lowest exited state of neon atom equals ≈16.6 eV [8], which exceeds the ionization potential of hydrogen atoms, the reaction

$$Ne^* + H_2 \rightarrow Ne + H_2^+ + e \tag{4}$$

will suppress successfully the radiation transitions in the mixture of neon and hydrogen gases. Using the same approximation as above, the intensity is now given by

$$I = \frac{kP_{Ne}}{P_0 + P_{Ne} + \alpha P_H}. \tag{5}$$

We see in Fig. 5 that Eq. (5) yields a good fit of the experimental data. The obtained value $\alpha \approx 30$ indicates that the process of Eq. (4) is 30 times more effective than Eq. (3), coming first from the difference of the average velocity of the molecules at the same temperature and next from the values of the cross-sections.

The pure hydrogen case is not as simple as the neon one. Here many new reaction channels appear and the light emission cannot be reduced to a one-step process as soon as the pressure is above a few Torr. First highly excited molecules may be dissociating. In that case, the excited atoms are created at supra-thermal velocities. In that case, as the coupling energy of a H_3^+ molecular ion is about 11 eV [7], the following reaction

$$H^* + H_2 \rightarrow H_3^+ + e$$

can efficiently decrease the population of the excited levels with principal numbers $n \geqslant 3$ ($E = 12.1$ eV) of hydrogen atoms in a dense gas. Taking for example the Hα line that has a decay rate of about 4.4×10^7 s^{-1} [6], the corresponding collisional decay rate may be estimated starting from a typical value of the cross-section derived from the molecule diameter $\sigma \approx 10^{-15}$ cm^2 [6,7]. This implies that, beyond a few torr, the frequency of atom collisions becomes larger than the probability of Hα radiation transitions, in accordance with the first part of the curve in Fig. 3. Non-dissociate molecular excited states have emission and destruction coefficients that are different from the atomic one. As the branching ratio for dissociation depends strongly on the initial vibro-rotational state of the molecule, this induces the emission and destruction coefficient to be pressure dependent. With a first order dependence, Eq. (2) may be replaced by

$$I = \frac{kP(1 + \alpha P)}{P_1 + P}. \tag{6}$$

In Fig. 3, the curve with a full line represents the result of Eq. (6), with $P_1 = 6.4$ and $\alpha = 9 \times 10^{-4}$.

4. Gas density gradient

When the source of emission of light is not uniform in density, a direct relation between the density and the light intensity can be obtained through the calibration described in the previous section, provided that the emission is local. Non-local emission may be due to large mean free path (mfp) either of the excited atoms or of the highest energy secondary electrons.

In our case, for atoms in excited states, the mfp is related to the lifetime of radiative states. If we

take the largest value of 100 ns for the lifetime of excited states, it yields 0.2 mm for the mfp of the hydrogen atoms at 300 K.

For high energy incident carbon ions, the maximum energy of the secondary electrons is $2m_eV^2$, with m_e the mass of the electron and V the velocity of the incoming carbon ions. Then, 60 MeV carbon ions yield a maximum of 10 keV for the energy of secondary electrons. In hydrogen, such electrons have large mfp but they are very few. The average value of the energy of the secondary electrons is $E_{av} \approx I \ln(E_{max}/I)$, I being the ionization energy and E_{max} the maximum of transferred energy. For hydrogen we get $E_{av} = 100$ eV. Thus most secondary electrons have enough energy to excite the target atom but their mfps are small enough not to perturb the gradient analysis. Using the data of [9], within a Monte-Carlo trajectory calculation, we obtain an mfp of 0.3 cm for 100 eV electrons in a 1 Torr hydrogen gas. Due to a much larger scattering cross-section the mfp in neon is much smaller. Thus non-local emission can perturb the gradient analysis only in the hydrogen case and at pressures less than a few torr.

One of the images of the gas ejection through the fast valves is shown in Fig. 6 (hydrogen). This figure attests that the emission is in fact almost local as the transverse radius of emission is nearly equal to the beam radius. The corresponding gas density profiles along the beam axis, deduced from these results, are reported in Figs. 7 and 8. They are reconstructed from the images of gas ejection, using the calibration procedure described in the previous section. The total linear density of the target is not more than 10^{20} cm^2. Therefore the 60 MeV carbon ions lost less than 10% of their energy within the target. The small induced variation of the excitation cross-section may be corrected by assuming a $1/E$ variation of the cross-sections. The saturation of the fluorescent yields at high gas density gives rise to a significant growth of inaccuracy in the reconstruction. In the considered diagram, the relative estimated error does not exceed a factor of two. Nevertheless, it might be considered to be acceptable for measurements of this kind.

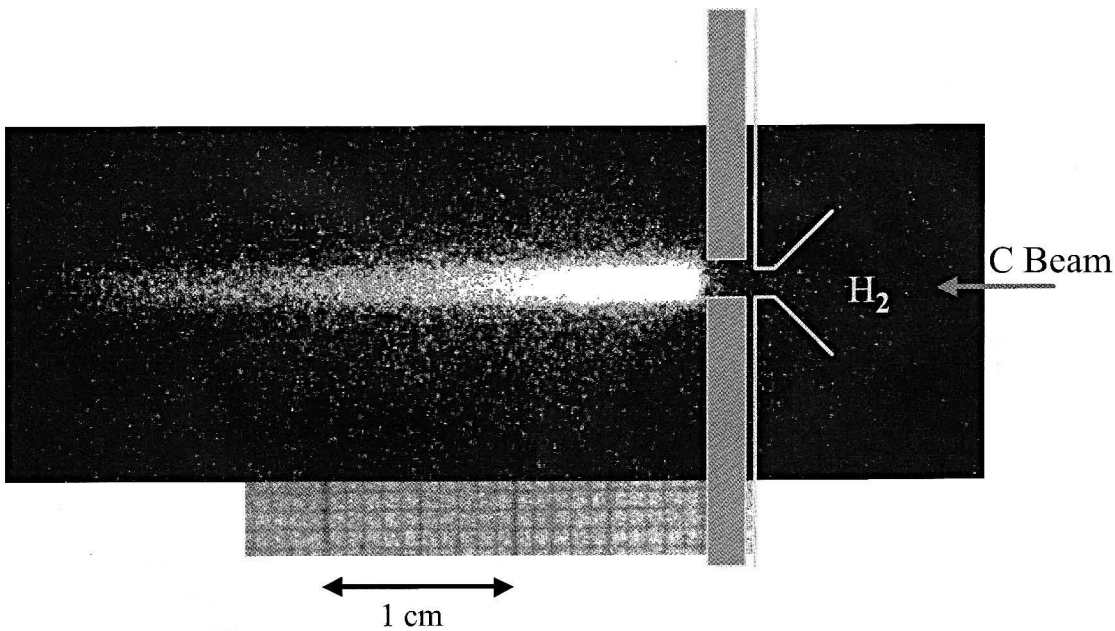

Fig. 6. Picture of the ejection area taken with the CCD camera. The drawing indicates the geometry of the aperture. The initial pressure in this case was 700 Torr of hydrogen flowing through a 2 mm hole.

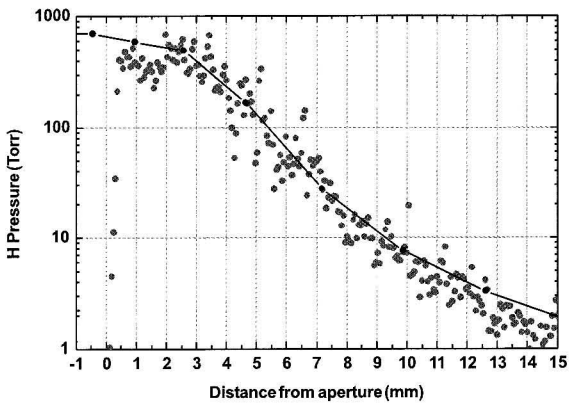

Fig. 7. Ejection profile for hydrogen. The solid line presents calculation from [10].

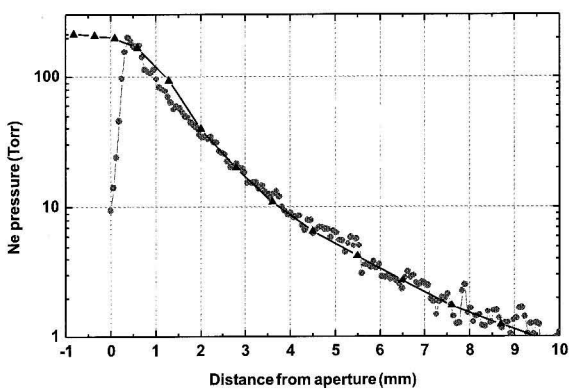

Fig. 8. Profile for neon ejection. The solid line presents calculation from [10].

The reliability of the results obtained are supported by a good agreement of the experimental data with the results of numerical simulation of gas leakage through a small aperture performed using a 2D hydrodynamic code (solid lines in Figs. 7 and 8). The gas flow was considered in the cylindrical geometry taking into account thermal conductivity and gas viscosity. The original equation set was solved in Lagrangian coordinates using a somewhat modernized numerical code [10] adapted to the experimental conditions.

In view of applications for density effect analysis in the beam–target interaction process, the important result that we obtain is that the linear density on the axis of the expanding gas is, at the maximum of the target operating pressure of nearly 3×10^{18} cm^2 in hydrogen and 10 times less in neon. For an energy loss analysis, it is necessary that the target linear density is much larger than these values. This is obtained by target of a few centimeters length at pressures of hundreds of torr. For charge state analysis, it will be required that the probability for one recombination process in the expanding gas is less than one. That is, the corresponding cross-section has to be smaller than the linear density.

Clearly these two conditions are related to heavy ions at high energies. Due to the large dependence of the recombination cross-section on the target atomic number, the hydrogen case is of more concern for charge analysis. A rough estimate of the domain of interest may be obtained using charge state equilibrium tables [11] and semi-empirical formula for the recombination cross-sections [12]. By requiring first that in its equilibrium state, the ion is still far from being fully ionized and next that the recombination cross-section is smaller than the linear density of the expanding gas we found, for example, that our device can be used at 2 MeV/u for atomic numbers from chlorine up to krypton. Above 4 MeV/u all ions have a small enough recombination cross-section, in that case it is thus only required that the equilibrium charge is not too large.

5. Conclusion

We present the complete package of experimental investigations to develop and to realize density diagnostics in a gas during its stationary regime of leakage in vacuum using fluorescence emission light from atoms exited by an incident ion beam.

The significant distinctions from linearity of the dependence of light yield on gas density even at relatively low pressure (5 and 50 Torr for hydrogen and neon, respectively) appears to be a strong evidence of the dramatic effect of the collision processes on the population of the exited levels and requires the mandatory predetermined calibration in the investigated range of gas pressures.

The obtained good agreement of the experimental and numerical data supports the capability of the technique proposed.

The abrupt transition between the gas container and the vacuum behind the aperture of the rotating valve observed in the experiment supported that the target proposed can be successfully used to investigate high density effects in ion stopping experiments of high energy heavy ions.

References

[1] G. Maynard, M. Chabot, D. Gardès, Nucl. Instr. and Meth. B 164–165 (2000) 139.
[2] H. Geissel, Y. Laichter, W. Schneider, P. Armbruster, Phys. Lett. A 88 (1982) 26.
[3] R. Bimbot, Nucl. Instr. and Meth. B 69 (1992) 465.
[4] C. Fleurier, J. Mathias, B. Dumax, J. Pellicer, A. Bonnet, D. Gardès, B. Kubica, Nucl. Instr. and Meth. B 61 (1991) 236.
[5] Princeton Instruments Inc..
[6] Yu.P. Rayzer, Physics of Gas Discharge, Nauka, Moscow, 1987.
[7] T. Tabata, T. Shirai, At. Data Nucl. Data Tables 76 (2000) 1.
[8] A. Hibbert, M. Le Dourneuf, M. Mohan, At. Data Nucl. Data Tables 53 (1993) 23.
[9] Z. Czyzewski, D. O'Neil MacCallum, A. Romig, D.C. Joy, J. Appl. Phys. 68 (1990) 3066, The cross-sections have been taken from http://web.utk.edu/~srcutk/Mott/.
[10] I Roudskoï, Laser Particle Beams 14 (1996) 369.
[11] K. Shima, N. Kuno, M. Yamanouchi, H. Tawara, At. Data Nucl. Data Tables 51 (1992) 173.
[12] A.S. Schlachter, J.W. Stearns, W.G. Graham, K.H. Berkner, R.V. Pyle, J.A. Tanis, Phys. Rev. A 27 (1983) 3372.